V.F. Andreev, A.S. Belousov, A.M. Fomenko,
L.A. Gorbov, T. Greenshaw, S.V. Levonian,
E.I. Malinovski, S.J. Maxfield, I.P. Sheviakov,
P.A. Smirnov, Yu.V. Soloviev, G.-G. Winter

A New High Energy Photon Tagger for the H1 - Detector at HERA

Moscow 2000

A New High Energy Photon Tagger for the H1-Detector at HERA

V. F. Andreev, A. S. Belousov, A. M. Fomenko, L. A. Gorbov
T. Greenshaw, S.V. Levonian, E.I. Malinovski, S.J. Maxfield**
*I.P. Sheviakov, P.A. Smirnov. Yu.V. Soloviev, G.-G. Winter***

Abstract

The H1 detector at HERA has been upgraded by the addition of a new electromagnetic calorimeter. This is installed in the HERA tunnel close to the electron beam line at a position $\simeq 8\,\mathrm{m}$ from the interaction point in the electron beam direction. The new calorimeter extends the acceptance for tagged photoproduction events to the high y range, $0.85 < y < 0.95$, and thus significantly improves the capability of H1 to study high energy γ-p processes. The calorimeter design, performance and first results obtained during the 1996-1998 HERA running are described.

* - *from Department of Phys. University of Liverpool, UK*
** - *from DESY, Hamburg, Germany*

The work is supported by the **INTAS-RFBR** grant, Project No **95-0679**

1 Introduction

The HERA accelerator at DESY brings into collision electrons (or positrons) with energy 27.5 GeV and protons with energy 920 GeV (820 GeV prior to 1998). A large proportion of the resulting interactions can be considered to occur between protons and essentially real photons, that is, photons for which $Q^2 \sim 0$, where $Q^2 = -q^2$ and q is the four-momentum of the photon exchanged between the electron and the proton. The energy, E_γ, of the photons in these photoproduction interactions can be related to the energies E_e and E'_e of the electron in the initial and final states through the expression

$$y = 1 - \frac{E'_e}{E_e} + \frac{Q^2}{4E_e^2} \simeq 1 - \frac{E'_e}{E_e} = \frac{E_\gamma}{E_e}.$$

Here y is defined by $y = p \cdot q / p \cdot k$, p and k being the four-vectors of the initial proton and electron, respectively. Measuring the energy of the outgoing electron enables the deduction of the photon's energy; the photon is then said to have been "tagged". In order to study the highest energy photon-proton collisons possible, a new electromagnetic calorimeter has been added to the H1 detector at HERA. This extends the range over which photons can be tagged from $0.3 < y < 0.8$ and $0.08 < y < 0.15$, using the electron taggers ET and ET44, respectively, to include the region $0.85 < y < 0.95$. In terms of the accessible photon-proton centre-of-mass energies, these regions correspond to $170 < W_{\gamma p} < 280$ GeV, $90 < W_{\gamma p} < 120$ GeV and $290 < W_{\gamma p} < 310$ GeV, respectively.

The electron taggers ET (or ET33) and ET44 are electromagnetic calorimeters located 33.4 m and 44 m from the interaction point (IP) in the electron direction, the negative z direction in the H1 co-ordinate system. The new calorimeter, the ET-8, is located at $z \simeq -8$ m from the IP to enable the measurement of electrons scattered with low energies while satisfying the constraints arising from the HERA machine: the space available for the ET-8 is limited and the environment hostile. This paper describes how the design of the ET-8 allows the triggering on and the measurement of low energy electrons with the necessary accuracy and ensures that it is sufficently radiation hard to survive operation at HERA. Test results are presented, as are the results of first physics studies using the ET-8.

2 Realization

2.1 Layout of H1 Lumi system

This technically challenging project requires the detection and accurate measurement of low energy electrons, down to 1.5 GeV, in a high radiation environment. The ET-8 must thus be radiation hard and have good energy resolution. In addition, its response to hadrons must be well understood to facilitate the separation of the signals due to electrons from those due to hadrons. Large hadronic background is expected due to the proton beam halo.

A plan view of the H1 luminosity system is shown in figure 1. Visible are the above-mentioned electron taggers, the ET and ET44, and the photon detector (PD). Electrons

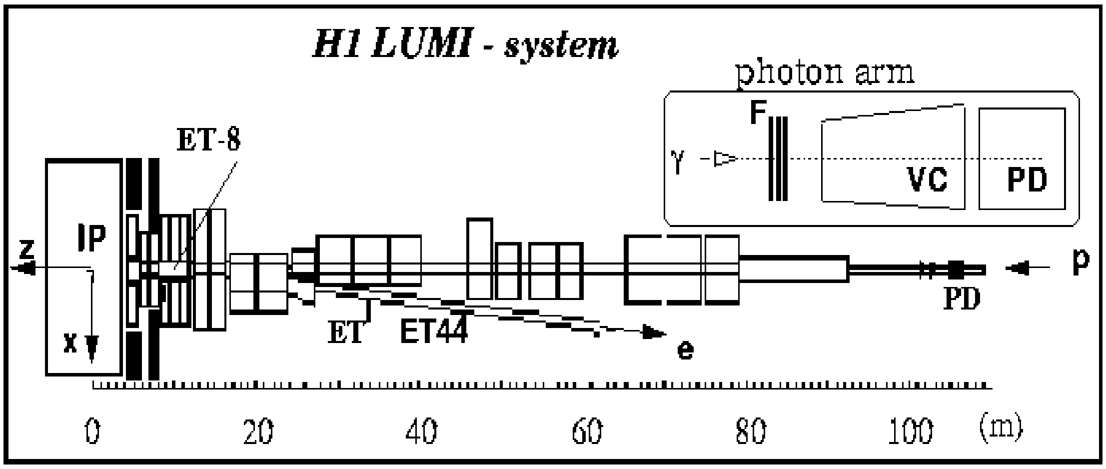

Figure 1: Schematic top view of the H1 luminosity system.

and photons originating from bremsstrahlung processes at the interaction point (IP) are emitted at very small angles and have to be detected in the luminosity system. The axis of the photon beam coincides with the axis of the incident electron beam which, under nominal operation conditions, coincides with the z-axis of H1. The bremsstrahlung photons propagating inside the proton beampipe leave it through an exit window at $z = -92\,\mathrm{m}$ and hit the photon arm of the luminosity system, of which the main part is the PD. The lead filter (F) and a water Čerenkov counter (VC) are located in front of the PD. The filter, of $2\,X_0$ thickness, absorbs most of the synchrotron radiation flux and protects the PD against radiation damage. At nominal luminosity, the direct synchrotron radiation flux carries a power of about 0.45 kW. The water VC acts as an additional $1\,X_0$ long active filter and can reject events in which a photon has converted between the exit window and the photon detector. It also provides an energy measurement for the absorped part of electromagnetic showers.

Accurate determinations of the luminosity are made using measurements of the e-γ coincidence rate within the acceptance of the luminosity system. Rapid luminosity monitoring during HERA running is provided by measurements of the rate of photons striking the PD, the so-called “single photon” method. The scattered electrons are detected in the electron taggers ET-33 and ET-44. These are total absorbtion Čerenkov calorimeters made of KRS-15 crystals [3]. The new detector was incorporated into the H1 trigger system and operated during all HERA luminosity running to allow the tagging of photoproduction events close to the HERA kinematical limit. The location with respect to the electron and proton beams and the dimensions of the detector must be accurately known in order to determine its acceptance with sufficient precision. An additional difficulty is that the space available for the ET-8 between the HERA beamline elements is very restricted.

2.2 Acceptance

Monte Carlo simulations for acceptance studies were performed using a fast simulation package H1LUMI [7]. This models the current HERA electron ring optics (the proposed spin rotators have yet to be included) as is described e.g. in [8] . Several possible positions for the new tagger were considered. After taking into account the apparatus currently

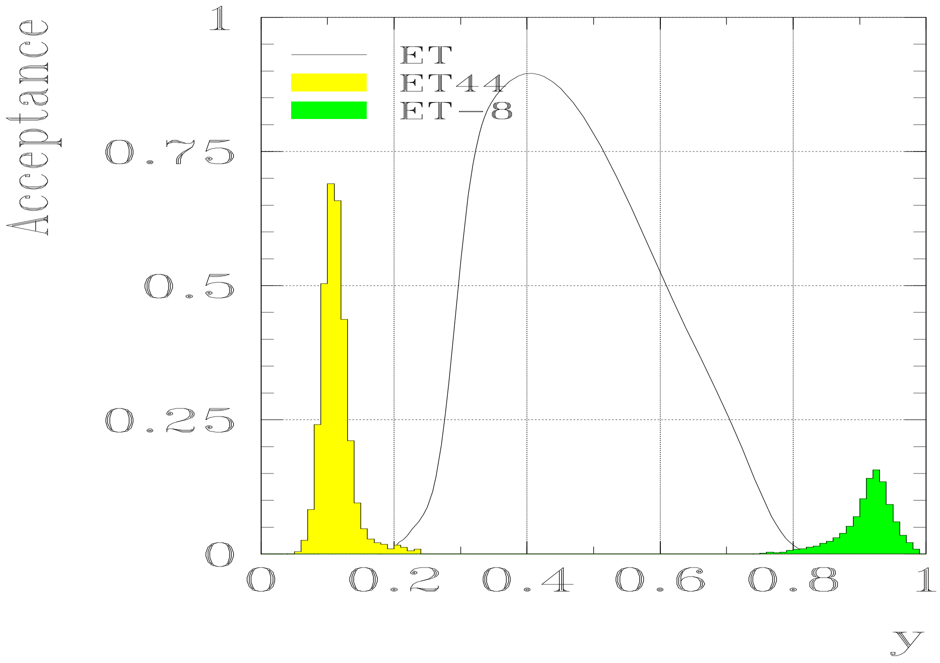

Figure 2: Acceptances of the three electron taggers for photoproduction with nominal electron beam conditions.

present in the HERA tunnel, the space needed for the calorimeter itself and the access requirements for installation and maintenence, it was decided to install the new tagger at the position $z \simeq -8\,\mathrm{m}$. Small possible variations of the beam parameters at the IP, horizontal and vertical tilts of ± 0.15 mrad and offsets of ± 1 mm, were taken into account in the simulation. These typically lead to 15 to 25% changes in the ET-8 acceptance. Precise knowledge of the tagger position with respect to the electron beam is thus very important. The acceptance can be defined with high precision from the data using $ep \to e\gamma p$ events, as is done for the present ET and ET44 calorimeters. This reduces uncertainties related to the precision with which real beam conditions can be simulated. Figure 2 shows the acceptances of the ET, ET44 and ET-8 for photoproduction with nominal beam conditions (zero tilt and offset). The ET-8 can be seen to extend the measurable y range to the high y interval $0.85 < y < 0.95$. The acceptance of the calorimeter depends on its position with respect to the electron beam axis, being most sensitive to the distance between the beam and the edge of the active calorimeter volume. The ET-8 acceptance shown here was calculated using the nominal separation of 4.5 cm.

The energy distributions of the electrons accepted by the ET-8 at various distances from the electron beam axis are shown in figure 3(a). The distributions are those for photoproduction with $Q^2 < 10^{-2}\,\mathrm{GeV}^2$.

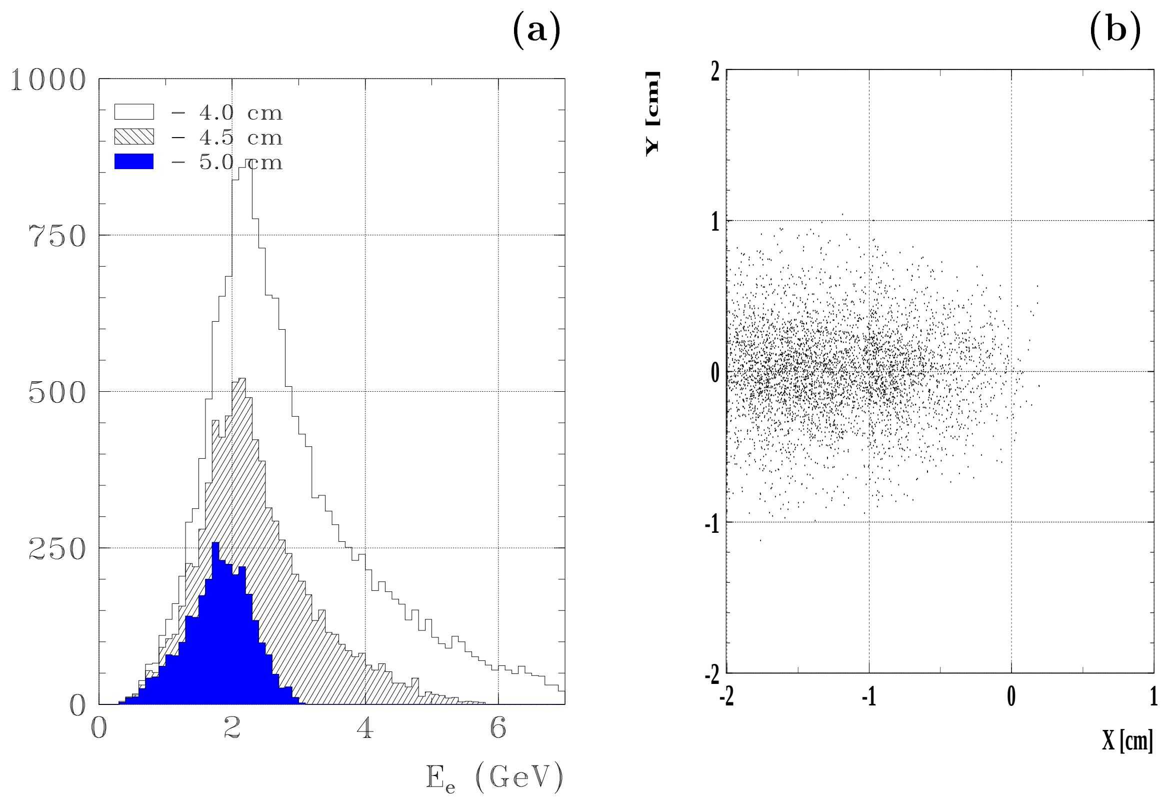

Figure 3: Energy and position distributions of the scattered electrons entering the ET-8: (a) energy distribution of the detected particles for various ET-8 e-beam axis separations; (b) distribution of co-ordinates of point at which electron enteres the front side of the ET-8.

The lateral size of the calorimeter was chosen on the basis of the transverse distribution of the accepted electrons at the front plane of the detector. This distribution is shown in figure 3(b). It is seen that the majority of events have entry points near the detector boundary close to the electron beampipe. Figure 3 illustrates that precise co-ordinate measurement is necessary for good reconstruction of the electron energy, allowing correction for those parts of the electromagnetic shower which leak out of the detector.

2.3 Detector design

Various technical solutions were investigated before a final decision was made on the calorimeter type. Possible choices included, total absorption calorimeters using KRS, NBW or PWO crystals, a lead-scintillator sampling calorimeter and a spaghetti type calorimeter. Although the combination of the total absorption crystal calorimeters and lead-scintillator calorimeters used in the existing H1 luminosity system, developed by the LPI group [4], has proved to be very successful, it was decided that a spaghetti calorimeter, as developed by H1 at DESY [5] was more suitable for the ET-8 detector. The SPACAL type calorimeters are built from arrays of scintillating fibres embedded in a heavy material, usually lead. The fibres inside these calorimeters transmit an amount of light which is proportional to the absorbed electromagnetic shower energy to a photo-sensitive readout device, for instance a photomultiplier (PM). If the transverse dimensions of the shower are considerably larger than the individual calorimeter cells, reasonably accurate determination of the shower position is possible. BICRON BCF-12 fibres of 0.5 mm

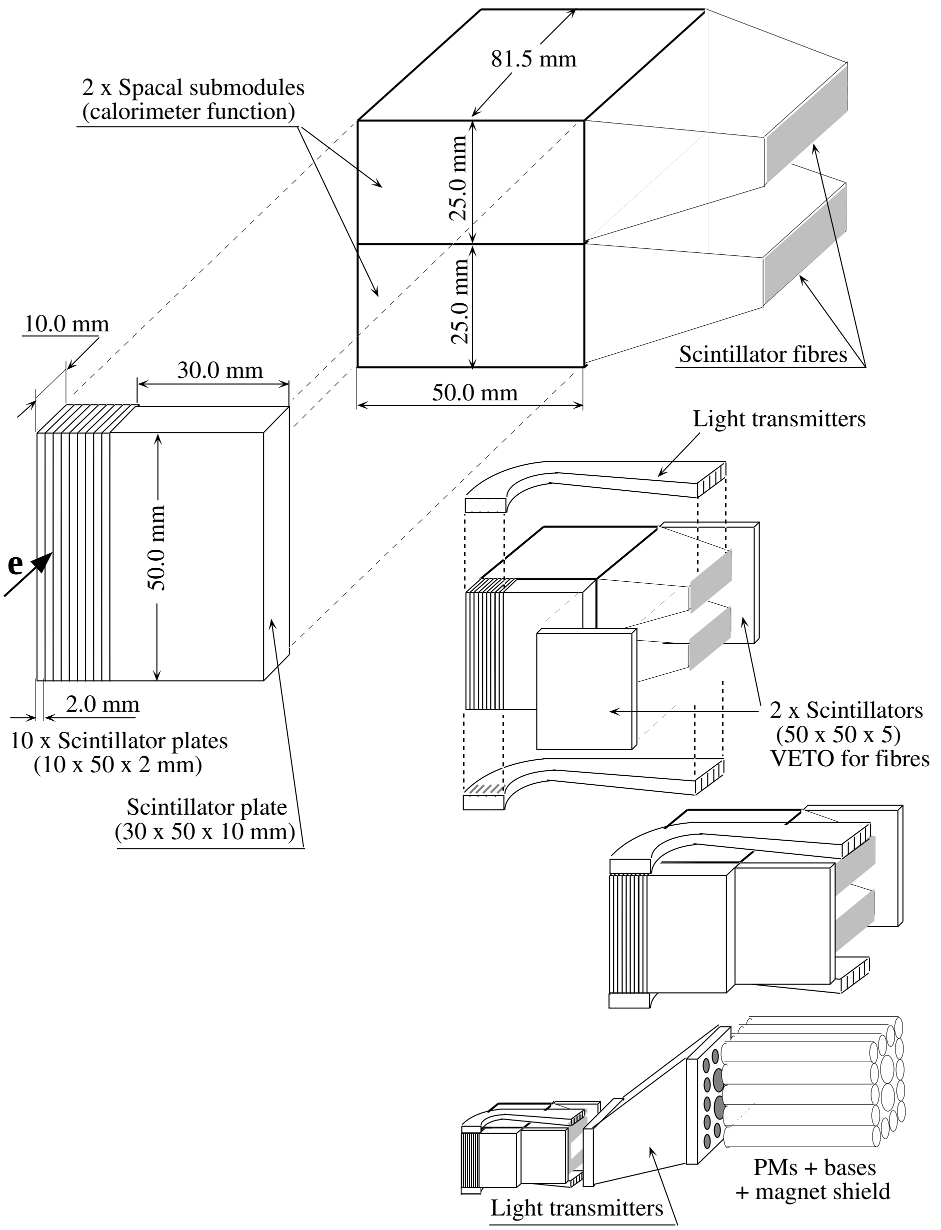

Figure 4: Design of prototype ET-8 (the ET-7).

diameter, which emit blue light with an emission peak near 430 nm, were used with a lead to fibre ratio of 2.3/1 by volume, giving a Moliere radius of 25.5 mm. This spaghetti type calorimeter has ~ 1.5 times better energy resolution than the total absorption crystal calorimeters mentioned above and the combination with a scintillator hodoscope provides the necessary spatial resolution.

A prototype of the ET-8 calorimeter, called the ET-7 as it was positioned about 7 m from the interaction point, was successfully tested during the July-October 1996 HERA running. Following these tests, the decision was taken to leave the ET-7 in place and it is now a permanent part of the H1 detector. Its design is shown in figure 4. The active volume of the ET-7 is 85 mm deep, corresponding to $10\,X_0$. The necessary horizontal spatial resolution is provided by the scintillator hodoscope placed in front of the calorimeter which allows measurement of the co-ordinate of the entry position of the electron with an accuracy of 1 mm using scintillator plates of thickness 2 mm. The vertical co-ordinate is determinated from the ratio of energies deposited in the two ET-7 modules. Two scintillator veto plates placed in front of and behind the scintillator fibres are used to provide background rejection. The amount of Čerenkov light from background particles in the light transmitters is orders of magnitude smaller than the signal from electromagnetic showers in the calorimeter due to the small lateral size of the light transmitters. Hence it is not necessary to shield these with additional veto plates. The detector was installed on a fixed support and stays permanently in the HERA median plane.

A schematic view of the ET-8 fibre detector, is shown in figure 5. The total longitudinal dimension of the active calorimeter volume is 92 mm. The calorimeter consists of three parts, the front tagging counter made as a spacal plate of $1.2\,X_0$ thickness, a central part and a rear co-ordinate plane. The central part, with cross section $40 \times 40\,\mathrm{cm}^2$ and of 70 mm length, corresponding to $9\,X_0$, consists of 4 modules. As in the majority of accepted events the electron hits the ET-8 close to the electron beam, the 3 modules closest to the beamline have a thickness of 6.7 mm, the module furthest away is thicker, thus optimising the accuracy with which the horizontal co-ordinate of the electron's entry point may be found. This is done by by comparing the energy deposited in the modules in the central part of the detector. The vertical co-ordinate is determined from the ratio of output responses of the upper and lower modules at the rear of the ET-8. Showers caused by particles which did not enter through the front of the detector are vetoed by requiring coincidences with signals from the front counter.

The level 1 trigger element for the new tagger requires the condition $E_{dep}^{tot} > E_{thr}$, where E_{dep}^{tot} is the total deposited energy in the calorimeter and E_{thr} the threshold energy which must have a low value, $E_{thr} \simeq 0.5 - 1.0$ GeV. For comparison purposes, a minimum ionizing particle deposits 50 MeV in the ET-8. An additional γ-veto condition from the photon arm of the luminosity system, no signal in the PD, suppresses the background from the high rate Bethe-Heitler process, $ep \rightarrow e\gamma p$, with an efficiency of $\sim 98\%$.

2.4 Radiation hardness of materials

The PD in the luminosity system is irradiated by the bremsstrahlung beam from electron-proton collisions and received a dose of ≈ 10 Mrad during the 1995 HERA running period

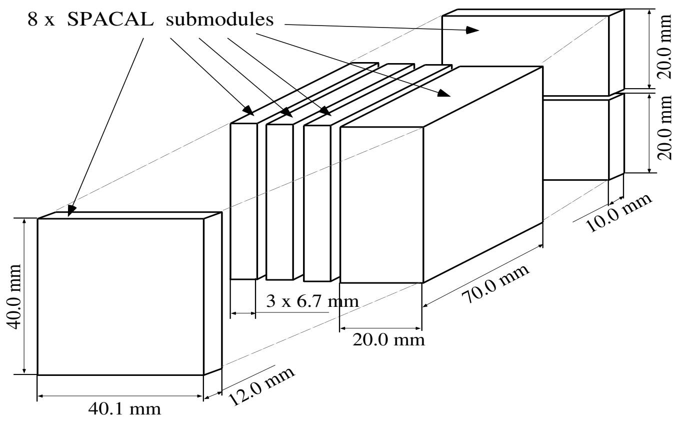

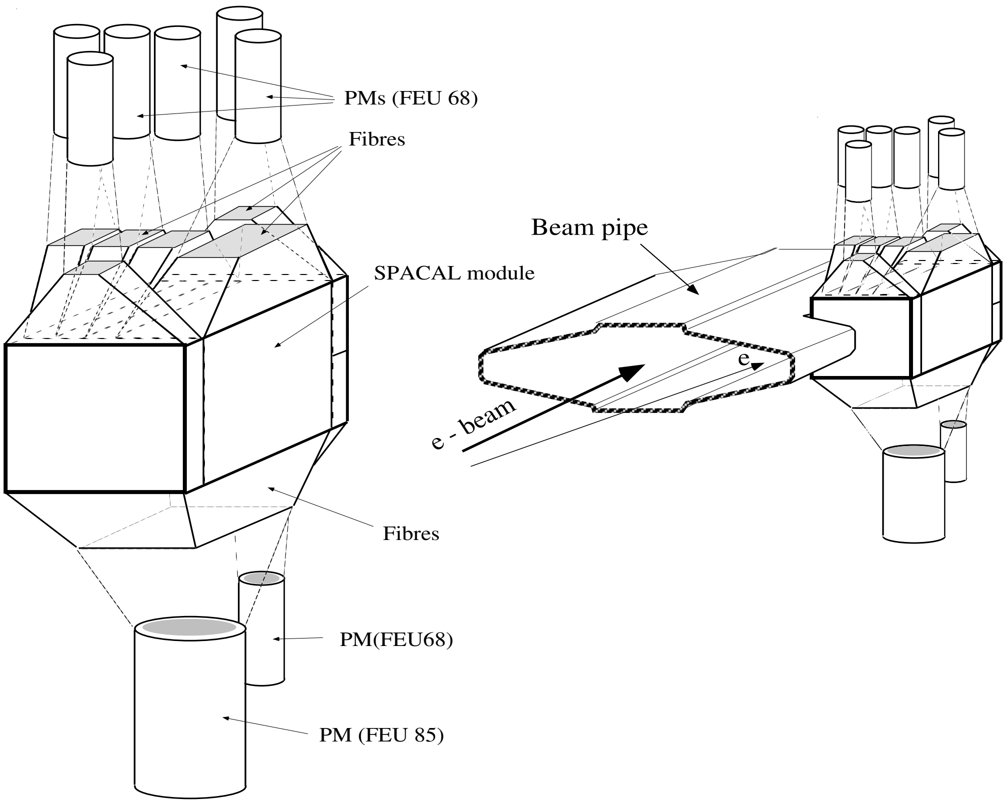

Figure 5: Design of the ET-8 calorimeter which was installed in the HERA tunnel in 1997

and other elements of the luminosity system also receive large radiation doses. The study of the radiation hardness of the materials used in the construction of the ET-8, the scintillators, fibres and plexiglass, is thus an important task. These studies were carried out at the 1 GeV electron synchrotron of the Lebedev Physical Institute in Moscow, Russia. The samples under study and several dosimeters were placed on the collimator

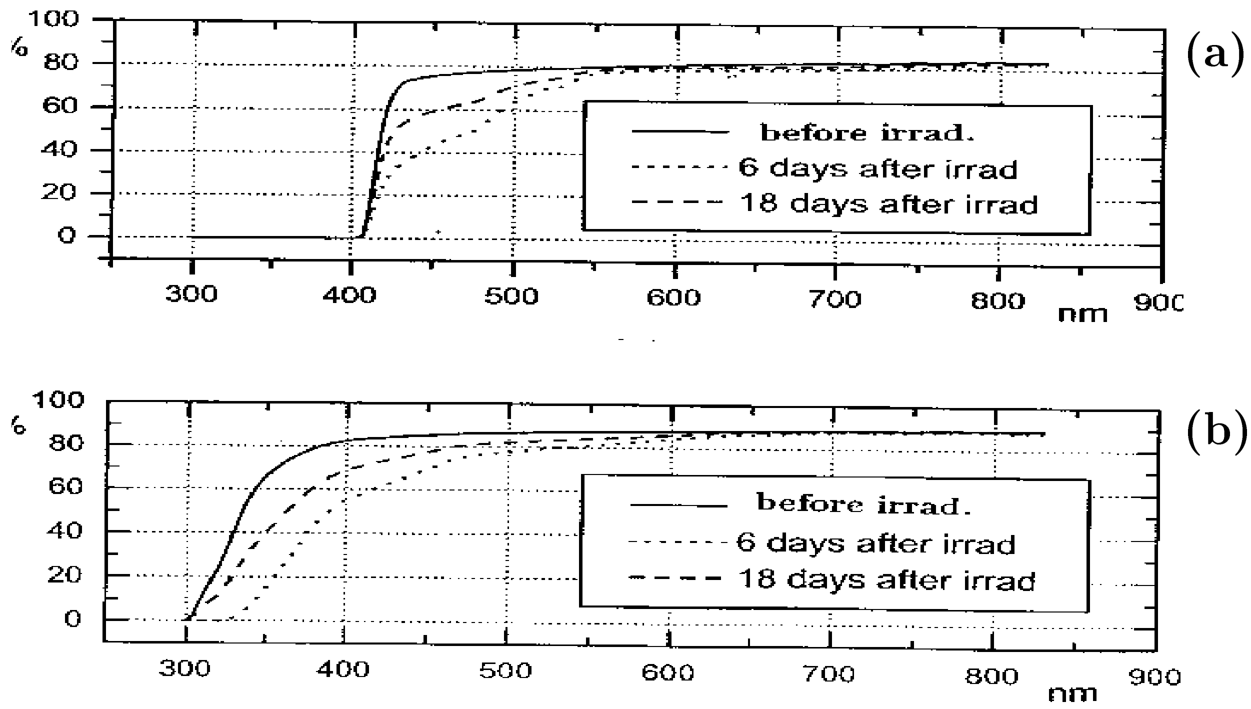

Figure 6: Optical transission of (a) scintillator and (b) plexiglass in the wavelength region $300 \leq \lambda \leq 800\,\mathrm{nm}$.

of the bremsstrahlung beam arising from the collision of the accelerated electrons with an internal target. After the exposure, the dosimeters were used to determine the dose delivered. The most important property studied was the change of the fibre attenuation length; the mean free path of photons in the fibre. Using the procedure described in [6], investigations were performed with BICRON fibres which had suffered a dose of 1 Mrad. The measurements show that the photon mean free path in the fibre decreased from $\sim$ 130 cm to $\sim$ 60 cm after irradiation. As the expected yearly doses resulting from luminosity running at the position of the ET-8 are about a factor of ten less than this, this effect is not large.

The scintillator and the plexiglass used in the light guides of the ET-8 were also studied. These were irradiated for about 40 hours and received a total dose of 2 Mrad. The scintillator sample then apppeared yellow in colour and the plexiglas brown, an effect which decreased with time after irradiation. The optical transparency of the samples before and after irradiation was measured using a spectrophotometer in the wavelength range 300 to 800 nm. The results are shown in figure 6. The changes due to the irradiation occur essentially in the short wavelength region. A slow recovery of transparency with time is also visible. Several days after the irradiation the optical properties were partly restored.

It should be noted that the total decrease in light yield due to the radiation damage of the active elements of the ET-8, the fibres, scintillators and plexiglass, does not influence the detector response or resolution significantly since the detector is continuously calibrated, as are all the detectors comprising the H1 luminosity system.

3 Test results

3.1 Event selection and event rates

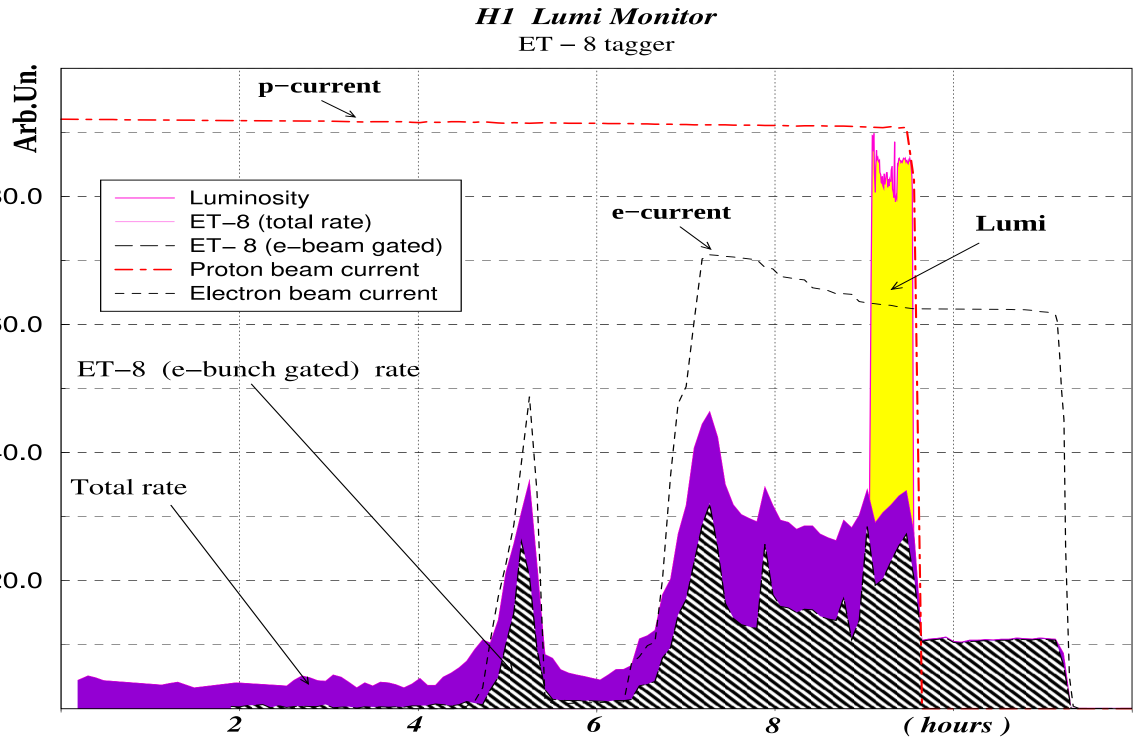

Figure 7: The event rate in the ET-8 for a range of beam and luminosity conditions.

The 1996 HERA running schedule originally foresaw a long shutdown in which it was planned to install a section of beampipe with an exit window in front of the ET-8. This schedule was modified, the long shutdown did not take place, so the new beampipe could not be inserted. The prototype ET-8 calorimeter was thus put into the HERA tunnel at a position as close to that foreseen for the ET-8 as possible. This was at about $z = -7$ m, so the prototype was dubbed the ET-7. Test results obtained using the ET-7 operation were presented in [9]. The installation of the new beam pipe and the ET-8 was performed in 1997.

Figure 7 shows, as a function of time t, the rates observed in the ET-8 during a luminosity run and the beam studies performed before and after that run. During the first 2 hours, HERA contained only a stable 920 GeV proton beam and the observed ET-8 rate is a consequence of the proton beam halo particles hitting the detector. At $t = 2$ hours, a low current electron beam was injected at an energy of 12 GeV and kept at this energy until $t = 5$ hours. A large part of the electron beam was lost at $t = 5$ hours during attempts to inject a higher electron current. At $t = 7$ hours, a high current electron beam was successfully injected at an energy of 12 GeV and then ramped up to 27.6 GeV. During this period the ET-8 rate contains the abovementioned proton beam induced component, but also a component resulting from the presence of the electron beam in HERA. Both electrons scattered off the residual gas in the HERA beam pipe and "off-momentum" electrons contribute to this component. Luminosity running was established at $t = 9$ hours. Soon after this the proton beam was lost, but the electron beam was kept for a further two hours. Hence, the final part of figure 7 shows the rate induced by the full energy electron beam alone. The measurements during luminosity running show clear evidence of an increased electron beam gated rate, whereas the proton beam induced component of the rate remains approximately constant. This figure illustrates graphically the problem that must be solved by the ET-8 and other luminosity system triggers. These must identify with high efficiency the events from electron-proton interactions while discarding as much as possible of the large background.

The time structure of the ET-8 signals was measured using flash analogue to digital converters. The averaged FADC pulse shape of the ET-8 response for the events triggered by the ET-8 trigger is shown in figure 8. Two spikes are visible in curve (a) on the figure. The first corresponds to proton halo particles hitting the ET-8, the second to the impact of electrons. The time between the two is 54 nsecs, as expected given the distance betwen the interaction point and the ET-8. This interpretation is confirmed by the results shown in curve (b) which was obtained when signals from other detectors were used to subtract events caused by proton halo particles. The timing information visible in figure 8 was used in the ET-8 trigger, described in more detail below.

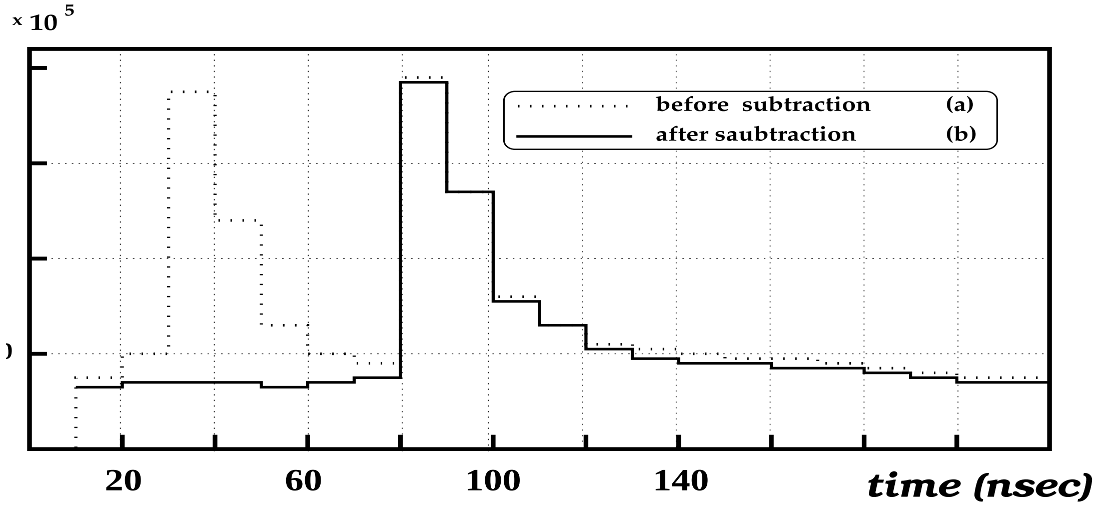

Figure 8: The averaged FADC's pulse shape for the events triggered by *H1 - ET-8* subtrigger: **a** - with proton halo and **b** - after subtraction proton halo.

In order to produce the level one trigger output for the ET-8 detector two independent conditions were combined. The first, the electron time window condition, was formed by requiring that the ET-8 signal occur within the time interval expected for electron-proton interactions. The second, the threshold condition, required that the energy in the ET-8 detector be more than E_{thr}. During the first stage of ET-8 operation, $E_{thr} \sim 1.0\,\mathrm{GeV}$.

3.2 Detector calibration

The calibration of the ET-8, and of all the detectors forming the luminosity system, is peformed using the Bethe-Heitler process $ep \rightarrow e\gamma p$. Since the energy transfer to the proton is negligible, the relation

$$E_{Tagger} + E_\gamma = E_e$$

must hold.

The ET-8 calibration procedure relies on the fact that the PD has already been calibrated, together with the main electron tagger (ET). In addition, the absolute energy scale of the PD can be determined using the high energy edge of the bremsstrahlung spectrum [10]. The first step of the calibration procedure is to select events with an impact

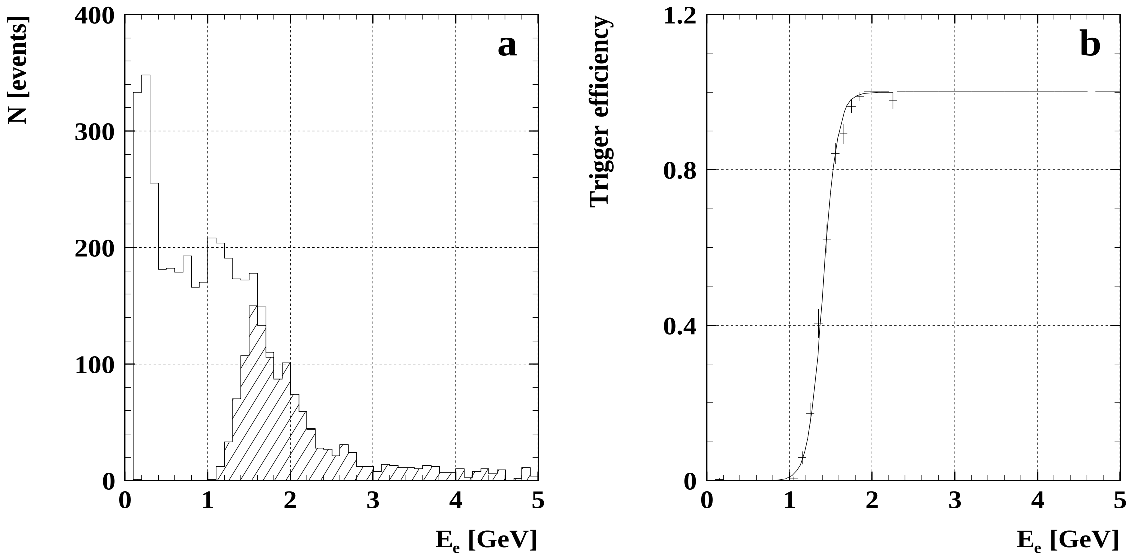

Figure 9: (a) Energy measured in the ET-8 for events which fired the level one ET-8 trigger (shaded histogram) and for a random trigger sample (open histogram); (b) efficiency of ET-8 trigger as a function of energy.

point in the front plane of the ET-8 which is well separated from the detector edges. The second step, described in detail in [11], determines the calibration coefficients $C(n)$ by minimizing the following sum:

$$\sum_i \Big(\sum_{n=1}^{N} C(n) * A_i(n) - E_e \Big)^2,$$

where N is the total number of channels, $A_i(n)$ is the amplitude of the signal detected in the n^{th} channel in the i^{th} event and $C(n)$ is the calibration coefficient for the n^{th} ET-8 channel. Using these calibration constants, the absolute energy spectrum shown in figure 9(a) was obtained. The shaded area represents the energy distribution of the scattered electrons in the ET-8 in events in which ET-8 trigger was set. It has a maximum around $\sim 1.5\,\text{GeV}$. The influence of the threshold $E_{thr} \sim 1.0\,\text{GeV}$ is clearly visible. The open histogram in the same figure contains all events taken by a random trigger. The background contribution peaks strongly at small energies. This background arises from off-momentum electrons in random coincidence with a signal from the main H1 detector. Comparing these two histograms allows the determination of the efficiency of the ET-8 trigger as a function of the energy detected in the tagger. This is shown in figure 9(b).

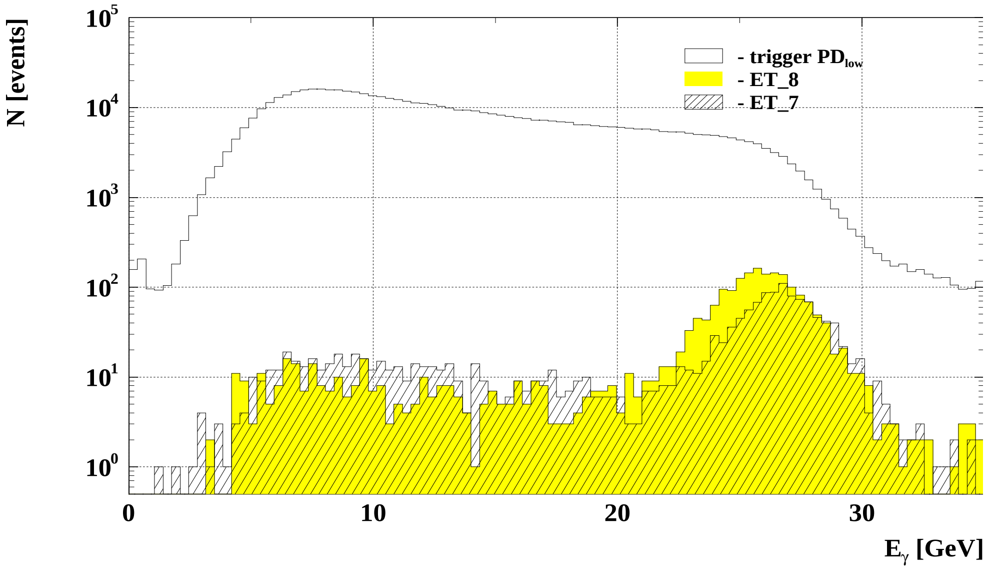

Figure 10: The photon energy spectra measured in the PD; the solid line shows that for all measured events, the shaded areas show the spectra for events triggered by the ET-7 and ET-8.

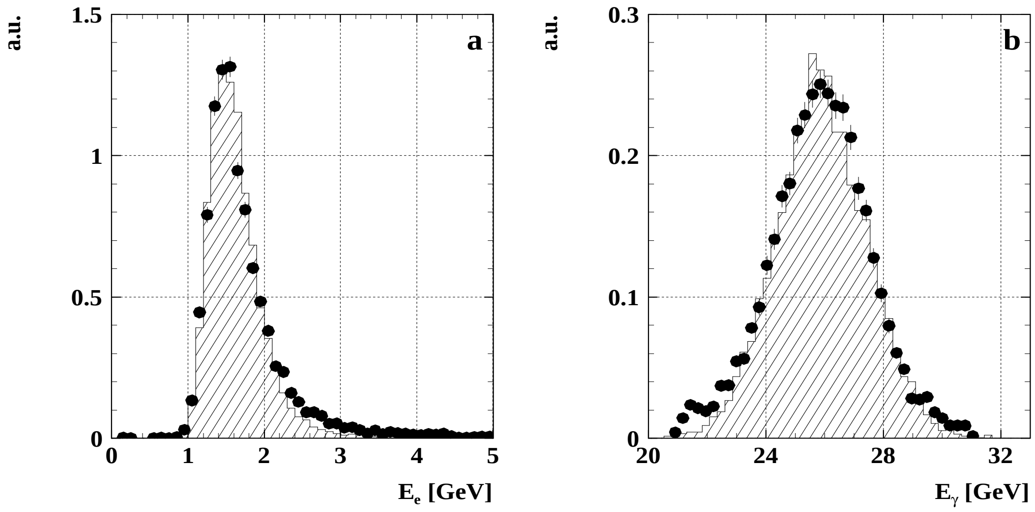

Figure 11: (a) The energy spectrum measured in the ET-8 (points) for bremsstrahlung events with a MC simulation (histogram); (b) The measured E_γ spectrum (points) in the PD for bremsstrahlung events in which the electron was detected in the ET-8, the MC prediction is shown as a histogram.

Figure 10 shows the measured energy spectrum of Bethe-Heitler photons in the PD. The solid line shows all measured events with significant energy in the PD. The shaded areas show the result of demanding coincidences with trigger signals from the ET-7 or the ET-8. The mean energies of these latter distributions are about 26.2 GeV for the ET-7 and 25.8 GeV for the ET-8, in agreement with the results of MC simulations for the average energy of bremsstrahlung photons inside the corresponding tagger acceptance.

The agreement between data and simulations is further demonstrated in figure 11,

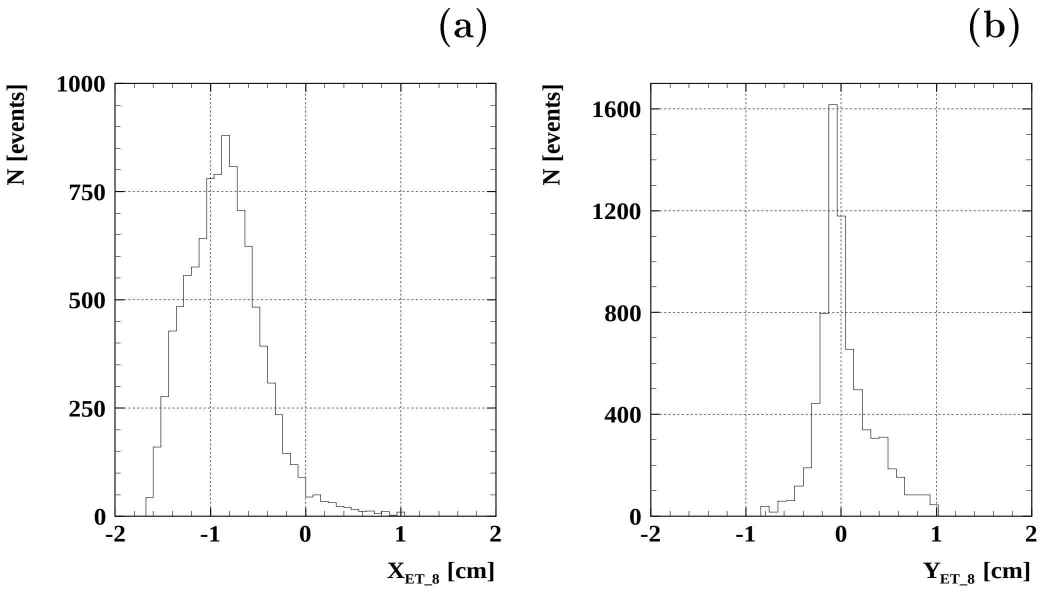

Figure 12: Distribution of the position of electrons scattered into the ET-8: (a) x co-ordinate of the detected particles at the tagger front plane; (b) y co-ordinate in the same plane.

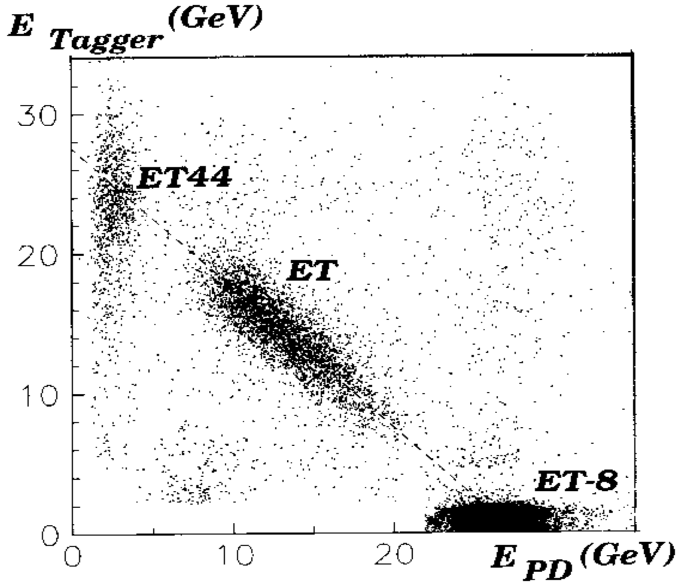

Figure 13: The E_γ - E_e correlation for bremsstrahlung events detected by the H1 luminosity system for the ET33, ET44 and ET-8.

in which the measured energy spectrum in the ET-8 tagger and the PD-detector for Bethe-Heitler events in which the electron was detected in the ET-8 are shown with the Monte Carlo predictions. The simulation includes the effects of detector resolution, trigger efficiency and pile-up.

The horizontal and vertical coordinates of the points at which electrons hit the front plane of the tagger are determined by comparing the energies deposited in the various modules of the ET-8. The reconstructed x and y co-ordinate distributions for a sample of data are presented in figure 12.

Figure 13 illustrates the correlation between the reconstructed electron energies E_{Tagger} and photon energies E_γ for bremsstrahlung events. These were selected by requiring a coincidence between the PD trigger and any of the electron tagger triggers. Due to the large difference in the trigger rates of the different taggers (ET44 $\simeq$ 280 kHz, ET $\simeq$ 170 kHz and ET-8 $\simeq$ 15 kHz at a luminosity of $5 \times 10^{30}\,\mathrm{cm}^{-2}\mathrm{s}^{-1}$) these data were taken with differing pre-scale factors for the various tagger triggers. The distributions of E_{Tagger} + E_γ are well described by a Gaussian function with the expected mean value of 27.6 GeV, the electron beam energy, and a standard deviation of $\simeq$ 1.3 GeV.

The event rates recorded by the different taggers within one electron fill (one luminosity run) are presented in figure 14. The observed rates in the various taggers are in good

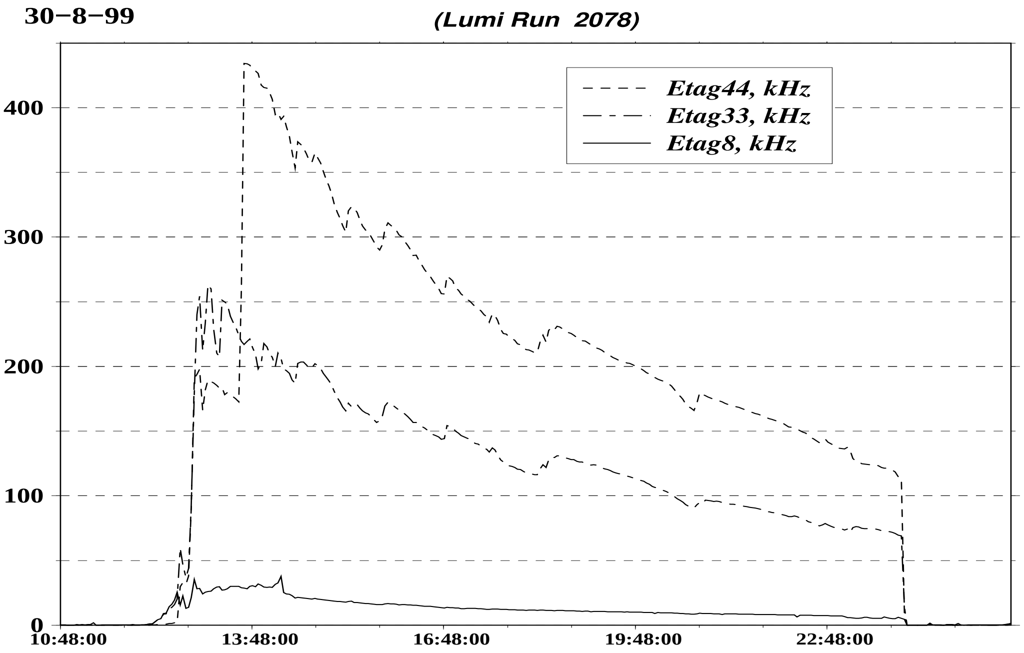

Figure 14: The behaviour of the rates measured in the various electron taggers during one HERA fill.

agreement with Monte Carlo simulations of bremsstrahlung events, taking into account the acceptance of the taggers. Note the sharp rise in the ET44 rate at the time the detector was moved into its working position close to the electron beam axis.

3.3 Physics results

The incorporation of the ET-8 into the H1 detector enables the identification of photo-production events at high $W_{\gamma p}$ and allows the accurate reconstruction of the interacting photon's energy. The energy distribution of the scattered electrons for candidate photo-production events is shown in figure 15. The MC prediction for this distribution is shown in the same figure. The Monte Carlo describes the data well. The data obtained using

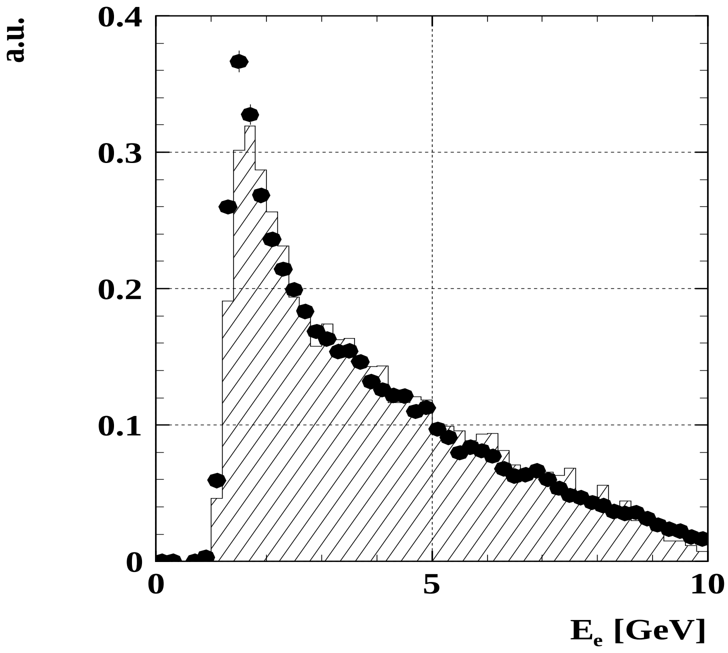

Figure 15: Electron energy spectra (points) measured with the ET-8 for photoproduction events, the histogram shows the MC prediction.

the ET-8 provide the basis for the study of many physics topics. As an illustration of the potential of the device, a preliminary measurement of the charged particle multiplicity in photon-proton interactions is presented here. This was made using minimum bias data collected by H1 in the autumn of 1997.

To study the energy dependence of the charged particle multiplicity in γp interactions, three data samples triggered by the three electron taggers were used. This provides a measurement in three $W_{\gamma p}$ regions, determined by the acceptance of the taggers, with average values of $\langle W \rangle = 100, 200$ and $290\,\mathrm{GeV}$.

The acceptances of all the taggers were determined from the data, using events from the Bethe-Heitler reaction $ep \to e\gamma p$ and the method described in [2]. The average charged particle multiplicity as a function of $W_{\gamma p}$ is shown in figure 16. Only statistical errors are given as the data are not corrected for the H1 tracker acceptance and efficiency.

The following criteria were applied in the analysis:

- Good quality runs were selected in which all the main components of H1 were fully operational, the central and forward trackers, the LAr and Spacal calorimeters, the electron taggers and the ToF system.
- The reconstructed event z-vertex was required to be within 30 cm of the nominal interaction point.
- A cut on y_{JB}, measured using the main H1 detector, was used to remove proton beam gas events as described in [2].

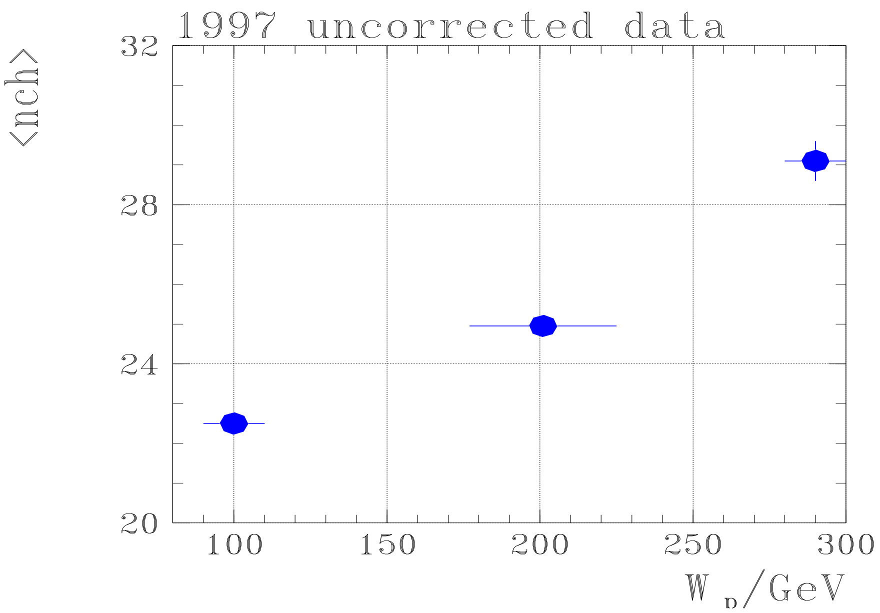

Figure 16: Energy dependence of the charged particle multiplicity in photoproduction.

The level of electron beam gas contamination (2 to 6%) was determined from pilot bunch studies and statistically subtracted.

To determine the event multiplicity, all vertex fitted charged tracks with $p_T > 0.15 GeV/c$ lying in the polar angular interval $15^\circ < \theta < 155^\circ$ in the laboratory system were used.

4 Conclusions

Following the investigation of various possible technical solutions, an extremely compact spaghetti type electromagnetic calorimeter, the ET-8, was built and installed within the H1 detector. This calorimeter makes possible the detection of electrons scattered in photoproduction interactions in which the photon takes a large proportion of the initial electron energy. Acceptance studies showed that the optimum position for the calorimeter, given the constraints imposed by the HERA machine, was at about 8 m from the interaction point in the electron direction. Studies of the materials used showed that they were able to withstand the high radiation doses to which they are subjected in their position close to the HERA beams. Tests of both a prototype calorimeter, the ET-8 and the associated trigger, reconstruction and calibration schemes have revealed that they function as desired. First preliminary physics results have been obtained.

5 Acknowledgements

We gratefully acknowledge the support of the DESY directorate and the machine group of the LPI synchrotron (Troitsk). Those of us from outside DESY wish to thank the

DESY directorate for the kind hospitality extended to us. It is also a pleasure to thank P. Biddulph and R. Eichler for active support and helpful discussions. We would like to thank INTAS, RFBR (grant INTAS-RFBR 95-0679) and the UK's PPARC for financial support.

References

[1] V.F. Andreev, P.S. Baranov, A.S. Belousov *et al*, "HERA Luminosity Measurement in H1 LUMI Monitor", LPI preprint N 28 (1993) Moscow.

[2] H1 Collaboration, "Measurement of the Total Photon Proton Cross section and its Decomposition at 200 GeV Centre of Mass Energy", Zeit. Phys. **C69** (1995) 27.

[3] V.F. Andreev, P.S. Baranov, A.S. Belousov *et al*, "Detectors of H1 LUMI Monitor", LPI preprint N 32 (1992) Moscow.

[4] H1 Collaboration, "The H1 Detector at HERA", DESY preprint H1-96-01.

[5] H1 SpaCal group, "Performance of an Electromagnetic Lead/Scintillating-fibre Calorimeter for the H1 Detector", DESY preprint, DESY-95-165.

[6] P.S. Baranov, A.S. Belousov, A.I. Lebedev and E.I. Malinovski, "Radiation Resistance of Materials used in Scintillation and Čerenkov Counters", LPI preprint N 53 (1996) Moscow.

[7] S. Levonian, "H1LUMI - A Fast Simulation Package for the H1 Luminosity System", H1 note H1-04/93-287 (1993).

[8] Brinkmann, "HERA Lattice and Optics Design", DESY HERA 92-07 (1992) 26.

[9] V.F. Andreev, A.S. Belousov, A.M. Fomenko *et al*, "Tagging High Energy Photons in the H1 Detector", Liverpool University Preprint PH 98-0901 (1998) Liverpool.

[10] N. Gogitigze and S. Levonian, "H1LUMI - An Offline Luminosity Determination for the 1995 e^+ Data", H1 note H1-0296-471 (1996).

[11] H1 Collaboration, "Experimental Study of Hard Photon Radiation Processes at HERA", DESY preprint DESY-95-024.